ACS Partner Journal

CHEM & BIO ENGINEERING

pubs.acs.org/ChemBioEng

Article

Biomass-Based Antibacterial Hybrid Engineering Hydrogel for Efficient Solar Steam Generation

Ping Wang, Xianjiao Wang, Xiaofei Wang, Xuliang Lin,* and Xueqing Qiu*

Cite This: *Chem Bio Eng.* 2024, 1, 252−263

Read Online

ACCESS | Metrics & More | Article Recommendations

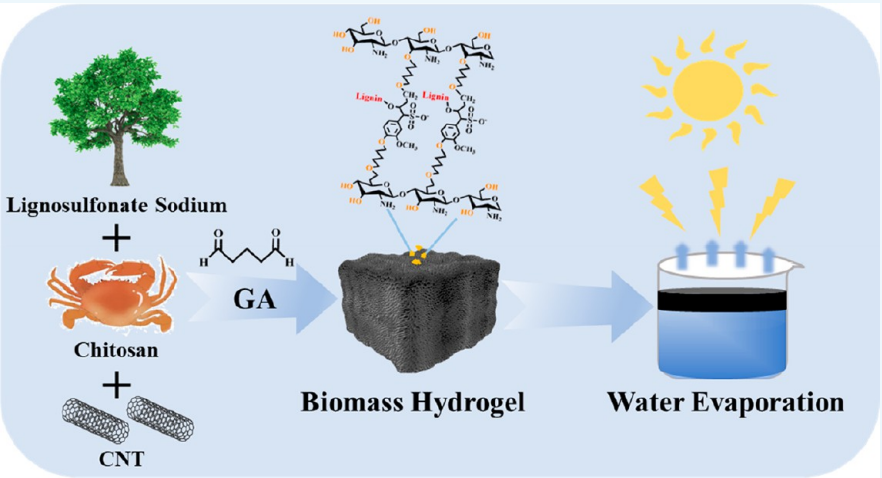

ABSTRACT: Interfacial solar steam generation is recognized as a promising solution to alleviate the scarcity of freshwater resources owing to its utilization of clean solar energy alongside its high efficiency and minimal heat loss. Nonetheless, the utilization of solar energy for water evaporation encounters challenges, primarily manifested in low evaporation rates and efficiency. Herein, we introduced an approach involving the development of a biomass-based hybrid engineering hydrogel evaporator, denoted as CLC (chitosan and lignosulfonate sodium hybrid hydrogel with a carbon nanotube). The construction of this evaporator involves the straightforward blending of lignosulfonate sodium (LS) and marine polysaccharide biomass chitosan (CS) with carbon nanotubes (CNT) serving as the photothermal materials. The interaction between the sulfonic group of LS and the amino group of CS with water molecules, facilitated by hydrogen bonding and electrostatic interactions, reduces the evaporation enthalpy of water, thereby lowering the energy demand for evaporation. Furthermore, the incorporation of LS reduces the thermal conductivity of the as-prepared hydrogel and promotes photothermal management to mitigate heat loss. The CLC hydrogel demonstrates an evaporation rate of 2.48 kg m^{-2} h^{-1} and energy efficiency of 90% under one sun illumination. Moreover, the CLC hydrogel exhibits excellent antibacterial properties (98.4%), ensuring that desalinated water meets drinking standards. This high efficiency and eco-friendly biomass hydrogel with antibiological pollution characteristics and purification abilities holds great potential for widespread application of long-term seawater desalination.

KEYWORDS: *lignosulfonate sodium, chitosan-based hydrogel, interfacial solar steam generation, desalination*

1. INTRODUCTION

Freshwater resources are decreasing due to climate change, environmental pollution, and population growth.[1,2] Terrestrial fresh water is naturally replenished through the hydrological cycle, which originates from ocean evaporation driven by solar energy.[3] However, due to the poor capacity of light absorption and large heat loss, the conversion efficiency of natural sunlight is just 30−45%.[4] In contrast, interfacial solar steam generation (ISSG) can achieve more efficient photothermal conversion and lower heat loss.[5,6] In recent years, a variety of broad solar spectrum absorbing photothermal materials have been developed, such as plasmonic nanoparticles,[7] semiconductors,[8] carbon materials,[9,10] and conjugated polymers.[11] However, these photothermal materials exhibit a lower evaporation rate

Received: December 21, 2023
Revised: February 27, 2024
Accepted: February 27, 2024
Published: March 4, 2024

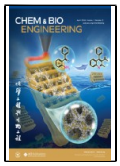

(<2.0 kg m^{-2} h^{-1}) under one sun illumination, attributed to the intrinsic high energy requirement of water vaporization escape.[12] Therefore, altering the state of water within the evaporators to decrease the evaporation enthalpy emerges as a pivotal strategy for substantially enhancing the evaporation rate.[13]

Hydrogels can reduce the energy demand for steam generated by water vaporization escape,[14] which overcomes the contradiction between the large energy consumption of water evaporation and the relatively low solar energy input of natural sunlight. The functional groups, such as hydroxyl (−OH), sulfonic acid ($-SO_3H$), carboxyl (−COOH), and amino ($-NH_2$) in hydrogels, can combine with water molecules through hydrogen bonds and electrostatic interactions.[15,16] It could be attributed to the interaction between water and the polymer network, wherein water molecules are ensnared by polar groups on the polymer chain to form a hydrated polymer network.[16] This hydrated polymer network generates intermediate water, known as activated water, which can evaporate with lower energy compared to free water.[17] Therefore, a more efficient ISSG can be reached by combining the selected photothermal materials and the designed structure of the hydrogel evaporator. Until now, numerous hydrated polymers featuring polar functional groups have been specifically engineered for the production of hydrogel evaporators. For instance, He et al.[18] developed dual-functional Co-CAT evaporators characterized by high water permeation and a reduction in evaporation enthalpy. Additionally, Yu et al.[19] proved that the chitosan (CS) polymer network exhibited low evaporation enthalpy of water and promote water evaporation in ISSG. Moreover, CS has excellent biological properties, such as nontoxicity, biocompatibility and biodegradability,[20] which makes it an ideal material for ISSG and will not cause secondary pollution to the environment. However, chitosan hydrogels have some disadvantages, such as low mechanical strength and high brittleness.

Lignin is the second most abundant biomass resource in nature, after cellulose. It contains abundant functional groups such as hydroxyl, carboxyl, and carbonyl groups,[21,22] which acts as cross-linking sites to establish a stable polymer network. The composite material consisting of lignin and polymer exhibits superior mechanical properties.[23,24] In addition, due to the abundant aromatic rings and conjugated structures in lignin,[25] the strong conjugation and $\pi-\pi$ stacking interaction can be found, which endows lignin with unique optical properties, including ultraviolet absorption and photothermal conversion potential.[26] Polymers with sulfonic acid groups easily increase the content of intermediate water by interacting with water. Therefore, lignosulfonate sodium (LS) rich in sulfonic groups becomes a potential material for preparing hydrogel evaporators.[27] Meanwhile, the sulfonic groups in LS can inhibit the adsorption of bacteria and show good antifouling performance.[28] However, as a major byproduct of paper-making and biorefinery, despite global annual production exceeding 60 million tons, lignin has yet to be fully leveraged to realize its full potential in high-value applications.[29,30]

In this study, LS and CS were used to form a chemically cross-linked hydrogel with a strong structural hydrogel network. The addition of carbon nanotubes (CNT) with broad-band absorption capacity were introduced, which provides the composite hydrogel excellent absorption ability in the whole spectral range. The sulfonic group in LS and the amino group in CS increase the content of intermediate water by interacting with water to form a hydrated polymer network and thus reduce the evaporation enthalpy of water. In addition, the hydrogel evaporator exhibits excellent salt tolerance and photothermal antibacterial ability, which shows great potential for long-term stable seawater desalination and the production of fresh water. In this study, the development of high-value utilization of biomass resources, i.e., lignin and chitosan, is of great significance to reduce carbon emissions and improve the environmental friendliness of hydrogel evaporators.

2. EXPERIMENTAL SECTION

2.1. Materials. Lignosulfonate sodium (LS) was supplied by Jilin Mya Import and Export Co., Ltd. The molecular weight of LS is 3200 g mol^{-1}, and the content of Na is 10%. Chitosan (CS, Mw =200000 g mol^{-1}, 90% degree of deacetylation) was purchased from Shanghai Macklin Chemical Co., Ltd. 3-Chloro-2-hydroxypropyltrimethylammonium chloride (CHPTMAC, 60%), sodium hydroxide (AR, 96%), and glutaraldehyde (AR, 50%) were purchased from Shanghai Aladdin Chemical Co., Ltd. Acetic acid (GC, 99.8%) was purchased from Shanghai Macklin Chemical Co., Ltd. Carbon nanotube (CNT, 5%) was purchased from Dongguan Keluder Technology Co., Ltd.

2.2. Preparation of Quaternized Lignosulfonate Sodium. LS (14.42 g) was dissolved in 90 mL of NaOH aqueous solution (∼20 wt %), and then 12.02 g of CHPTMAC was drop-added into the LS solution under stirring. After that, the mixture solution was stirred at 85 °C for 4 h, and finally the obtained quaternized lignosulfonate sodium (QLS) solution was purified by dialysis and then freeze-dried to gain QLS powder.

2.3. Preparation of Lignosulfonate Sodium-Chitosan Composite Hydrogel. First, 0.15 g of CS was dissolved in 5 mL of acetic acid solution (1 wt %), stirred for 5 min to completely dissolve. Then, 0.10 g of QLS was dispersed into 3 mL of acetic acid solution (1 wt %). Third, the LS solution was slowly dripped into the CS solution and stirred for 2 h to dissolve the two substances into a uniform solution. A certain amount of CNT was added to the homogeneous solution. The glutaraldehyde solution of 3 mL (1 wt %) was quickly dripped after dissolving uniformly, and the surface bubbles were removed by ultrasound. Finally, the CS/LS-CNT (CLC) hydrogel was obtained by static reaction of the solution in a cylindrical mold for 12 h. The crystallization rate of ice crystals was controlled by the liquid nitrogen freezing method to obtain uniform and regular pore structure of the hydrogel, and aerogel CLC was obtained after freeze-drying.

2.4. Material Characterization. The structure of functional groups before and after quaternization modification of lignosulfonate sodium was characterized by an infrared spectrometer (iS50R, USA). Nuclear magnetic resonance hydrogen spectrum of lignosulfonate sodium before and after quaternization modification was characterized by a nuclear magnetic resonance spectrometer (Bruker,AVANCE III HD 400).

The molecular structure of chitosan and its hydrogel was characterized by X-ray photoelectron spectroscopy (Thermo Fisher, Escalab 250Xi). The surface morphology of freeze-dried hydrogels was observed by focused ion beam scanning electron microscopy (SEM, LYRA 3 XMU, Czech Republic). Fourier transform infrared (FTIR, iS50R, America) spectroscopy was used to detect the material in the wave number range 4000−400 cm^{-1}. The mechanical tests of hydrogels and the compressive stress tests were carried out, respectively, on the mechanical properties rheometer platform (MCR301, Austria) and the universal testing machine (Inspect Table Blue 5KN, Germany). The water contact angle (WCA, OCA100, Germany) was used to evaluate the wettability of the aerogel. The thermal conductivity of the aerogel was characterized by a hot disk (TC3000e) based on the transient hot wire method. The reflectance and transmission spectra (250−2500 nm) of the aerogel were collected by a UV−vis−NIR, (UV-3600Plus, Shimadzu) spectrophotometer. The enthalpy of evaporation of water in the hydrogels was determined by TG-DSC (STA409PC). Raman spectra of water in aerogel networks were recorded on a spectrometer

https://doi.org/10.1021/cbe.3c00121
Chem Bio Eng. 2024, 1, 252−263

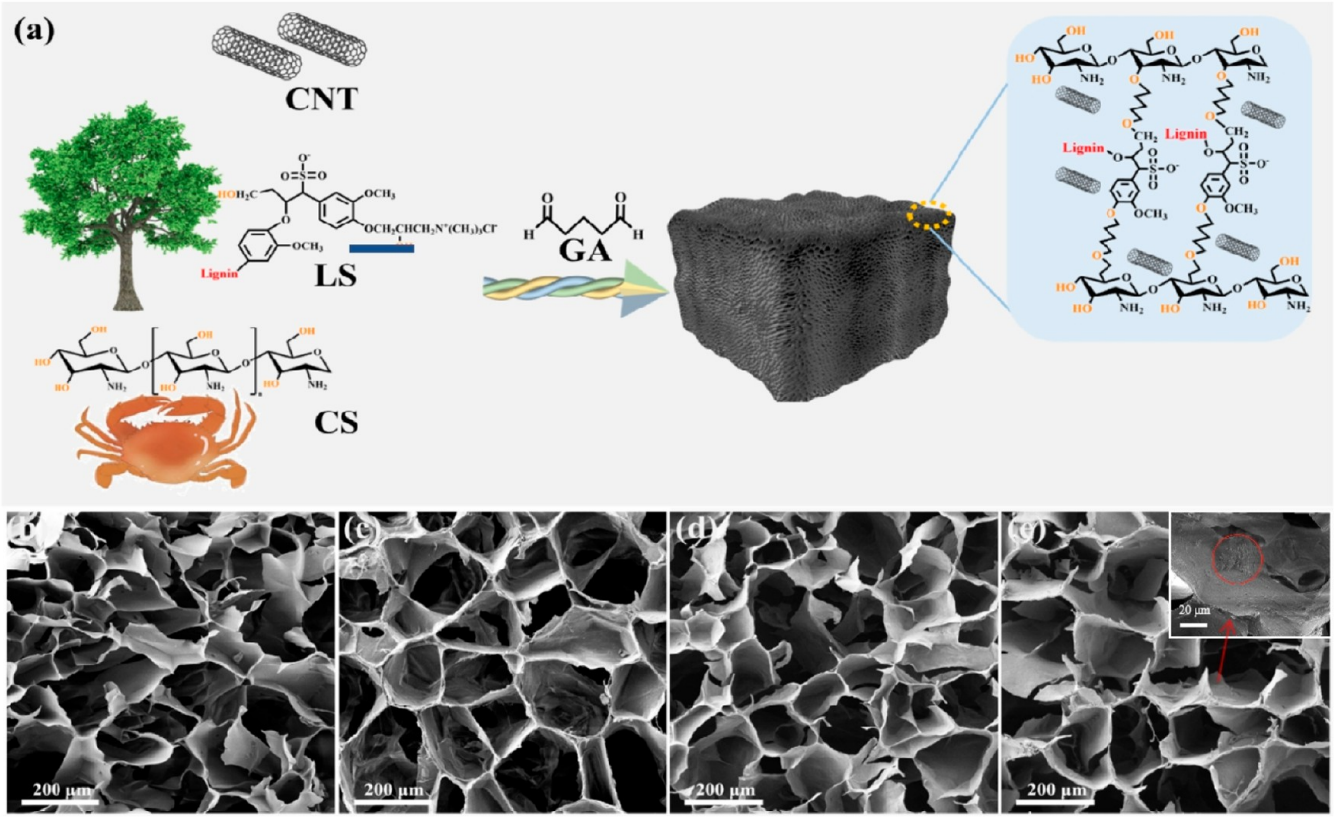

Figure 1. (a) Synthesis schematic of sodium lignosulfonate-chitosan-based hydrogel. SEM images of (b) CS aerogel, (c) CL aerogel, (d) CS-CNT aerogel, and (e) CLC aerogel.

(LabRAM HR Evolution, France) with an excitation wavelength of 532 nm. The methylene blue (MB) concentration was determined by an ultraviolet spectrometer (UV-2600i, Japan).

2.5. Antibacterial Assay. The antibacterial activity of hydrogels against *Staphylococcus aureus* (*S. aureus*, ATCC 29213) was investigated by using the spread plate method. Typically, hydrogel pieces with a diameter of 10 mm were first presoaked in PBS until reaching absorption equilibrium. Subsequently, they were sterilized with a UV lamp for 30 min and then immersed into a bacteria suspension (1 mL, 1.0×10^8 CFU/mL). After coincubating at 37 °C for 4 h, these samples were treated with NIR irradiation (808 nm, 1 W cm^{-2}) for 15 min. Afterward, the bacterial solution was taken out from hydrogels and diluted. Finally, the diluted bacterial suspension was spread onto the fresh broth Agar plate. After cultivation overnight, the bacterial colonies on the Agar plate were photographed. The bacteria suspension treated by PBS without hydrogel samples was considered the control group.

Besides, we studied the antibacterial properties of hydrogels by a bacterial live/dead staining assay. Briefly, after different treatments, the bacteria cells were costained by PI and SYTO9 for 20 min in the dark, followed by washing thrice with PBS. All bacteria were labeled by SYTO9 and appeared with green fluorescence, while dead bacteria were stained by PI and revealed red fluorescence. Finally, fluorescence images were captured by using confocal laser scanning microscopy (LSM 800 with Airscan, Carl Zeiss, Germany).

2.6. Solar Evaporation Experiment. Solar steam generating experiment is conducted in a laboratory self-made device; the device is equipped with solar light simulator (CEL-HXF300-T3, China), used to determine the additional solar irradiation power density detector (TES-1333, China), an infrared camera for measuring the surface temperature of hydrogels (UTi220A), and an electronic balance for monitoring changes in water quality (OHAUS, PX224ZH, USA). The sample floated on the surface of the glass container, and white foam covered the surface that was not covered by the hydrogel. A solar simulator is then used to illuminate the sample at one solar illuminance (1k Wm^{-2}). The room temperature in the laboratory is controlled at ~22 °C. The humidity during the indoor water evaporation was controlled at 50%. The evaporation rate in 60 min was measured under steady-state conditions. The water evaporation rate was calculated by the following equation:[31]

$$\nu = \frac{dm}{s \times dt} \tag{1}$$

where m is the mass of evaporated water, s is the illuminated area, t is time, and ν is evaporation rate.

The energy conversion efficiency of the hydrogel evaporator is calculated as follows:

$$\eta = \frac{\nu \times \Delta H_{equ}}{C_{0\rho t} \times P} \tag{2}$$

where η is the energy conversion efficiency of the substance, $C_{0\rho t}$ is the optical concentration of the substance, and P is the sunlight intensity.

The evaporation enthalpy was calculated based on following equation:[32,33]

$$\Delta H_{equ} = \int_{t_0}^{t} q \, dt \tag{3}$$

where ΔH_{equ} is energy consumed for water evaporation, q is the heat flux characterized using DSC, and t is time.

The ion concentrations of simulated and desalted water were measured by inductively coupled plasma mass spectrometry (ICP-MS, Agilent 7200S).

3. RESULTS AND DISCUSSION

3.1. Physicochemical Properties of the CS-LS Hydrogel. The schematic diagram of the preparation of a three-dimensional porous CLC hydrogel is shown in Figure 1a. The

https://doi.org/10.1021/cbe.3c00121
Chem Bio Eng. 2024, 1, 252−263

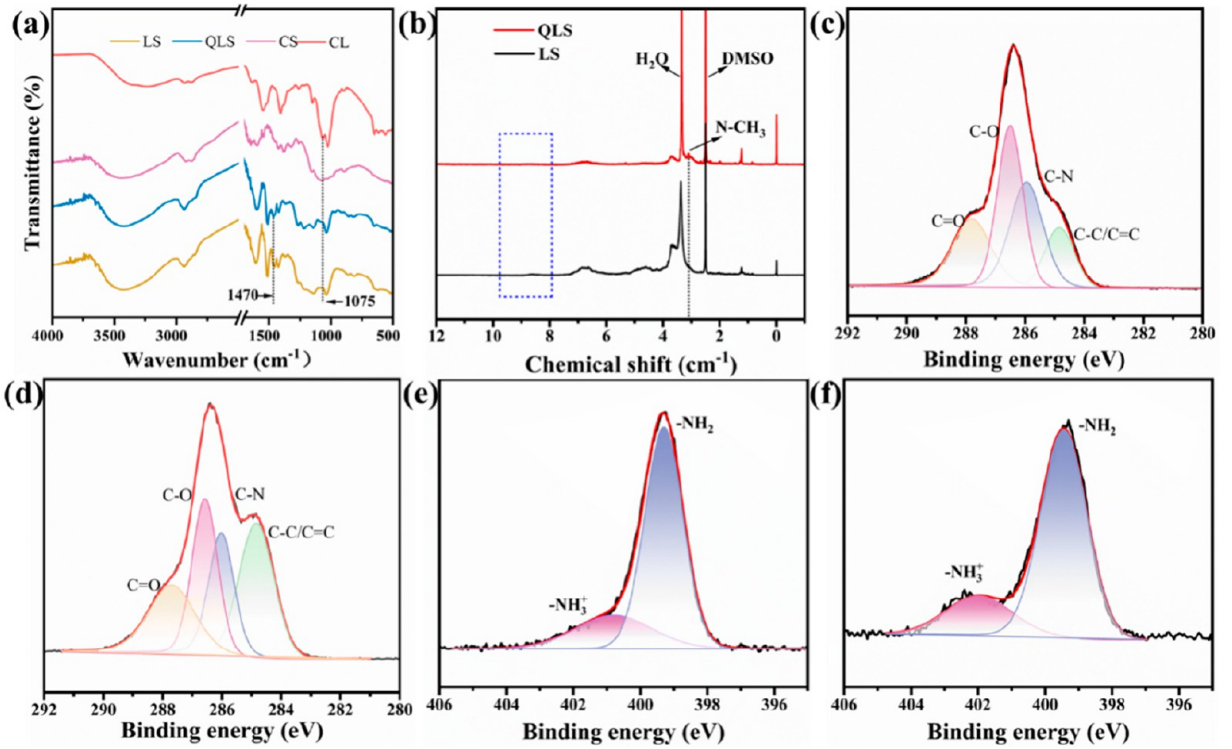

Figure 2. (a) FT-IR spectra of pure LS, QLS, CS, and CL aerogel. (b) ^{1}H NMR spectra of LS and QLS. XPS C 1s spectra of (c) CS and (d) CL aerogel. XPS N 1s spectra of (e) CS and (f) CL aerogel.

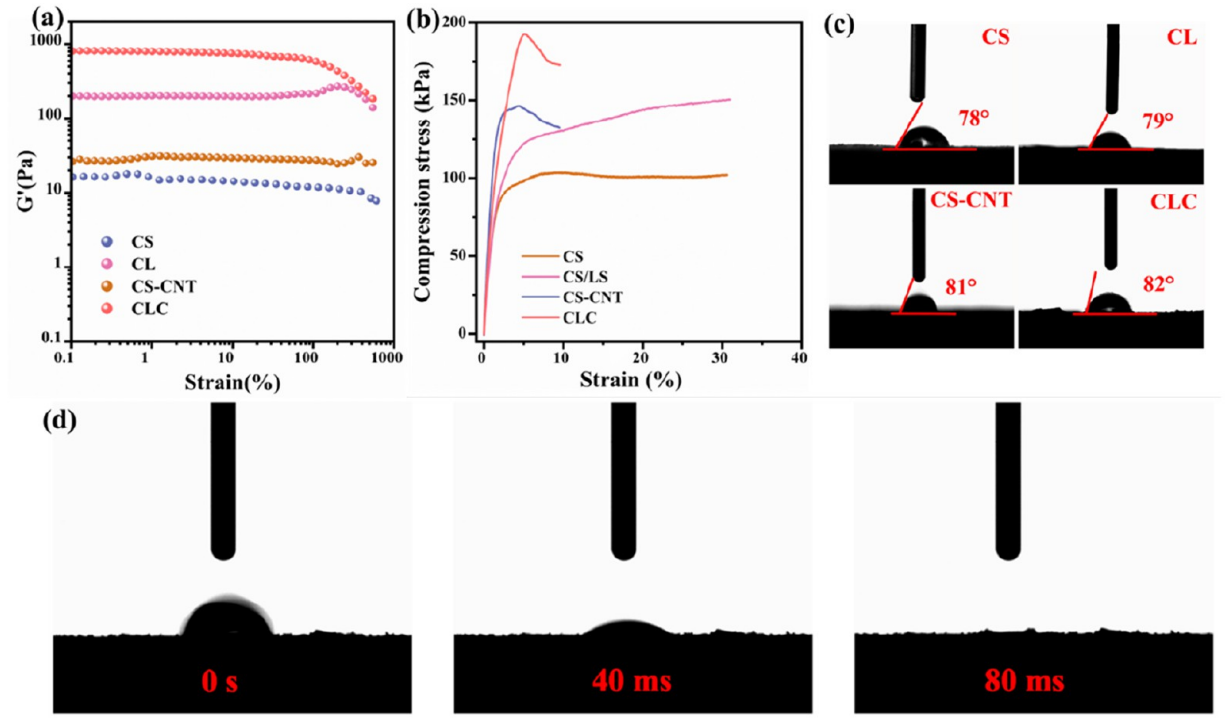

Figure 3. (a) Dynamic mechanical analysis for the storage modulus (G') and (b) compressive stress−strain curves of the CS, CL, CS-CNT, and CLC hydrogels. (c) Water contact angle measurements of the CS aerogel, CL aerogel, CS-CNT aerogel, and CLC aerogel. (d) Time evolution of the water contact angle of the CLC aerogel.

quaternary LS with increased electropositive property can be dissolved with chitosan to form a homogeneous solution, which cross-linked and copolymerized into CS-LS hydrogel (CL) under the action of glutaraldehyde. Then, based on the CL hydrogel framework, carbon nanotubes were uniformly embedded in the hydrophilic polymer network, and the black

https://doi.org/10.1021/cbe.3c00121
Chem Bio Eng. 2024, 1, 252−263

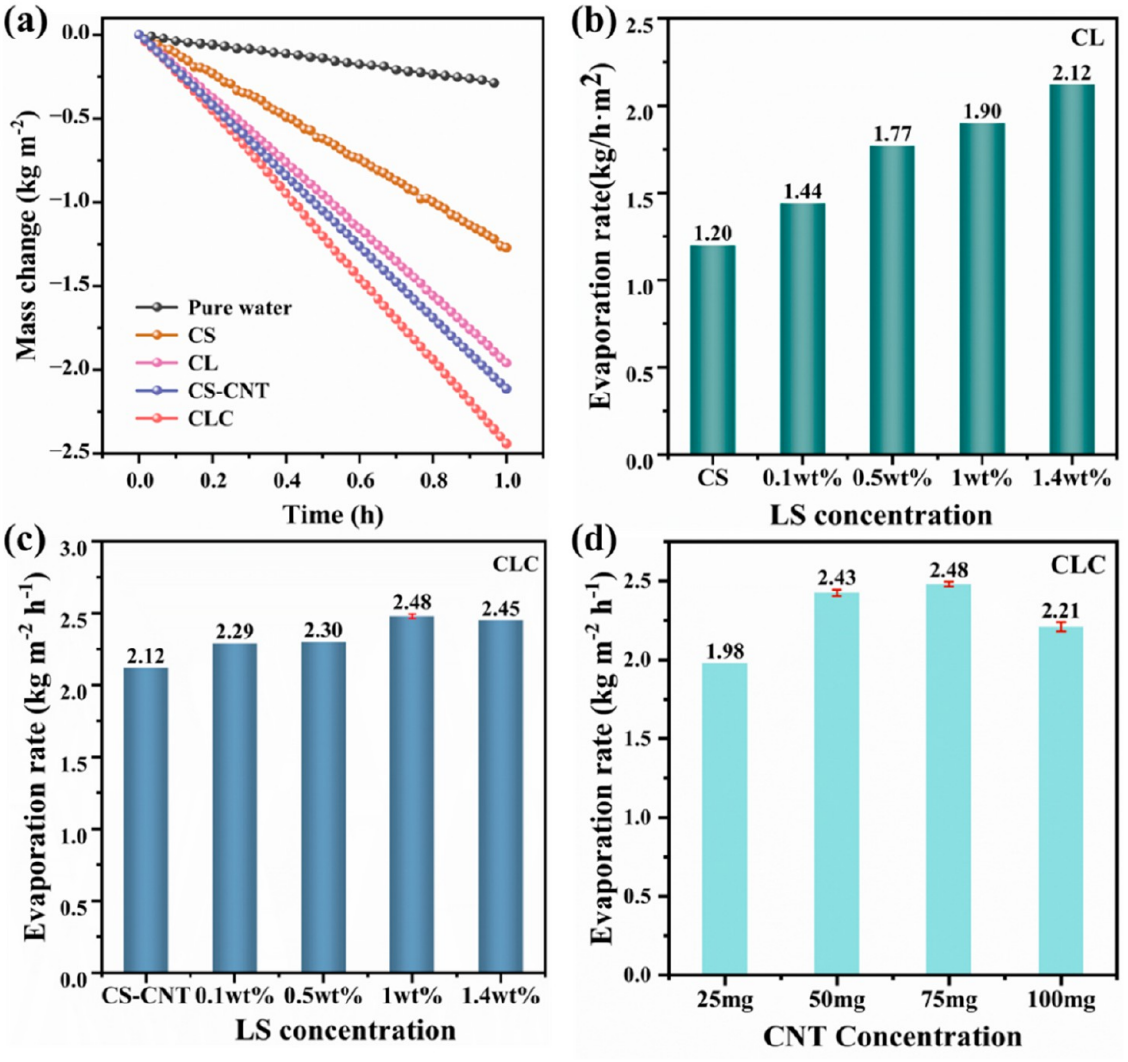

Figure 4. (a) Mass changes of pure water, CS, CL, CS-CNT, and CLC in pure water. Water evaporation rates of the CL hydrogels with different LS concentration. (b) Water evaporation rates of the CL hydrogels with different LS concentration. Water evaporation rates of the CLC hydrogels with different (c) LS concentration, and (d) CNT concentration.

CLC hydrogel was obtained by monolithic loading of CNTs. For comparison, the CS hydrogel (CS) and CNT-loaded CS hydrogel (CS-CNT) were prepared. As shown in Figure 1b, the CS hydrogel showed a thin sheet structure; the pore structure is broken, and there is no relatively regular channel. Moreover, similar results were shown in the CS-CNT hydrogels (Figure 1d). In contrast, the CL hydrogels exhibited interconnected macroporous structures with regular pore structures and no obvious structural fragmentation (Figure 1c), indicating that the addition of lignin could enhance the pore structure strength of the hydrogels and make them difficult to be broken. In addition, the CLC hydrogels showed consistent results with interconnecting pore structures and rough pore walls, and CNT is embedded in polymer hydrogel and distributed in channels and gaps. This interconnected porous structure imparts capillary action, facilitates water transport, and facilitates solar heat harvesting.[34]

The chemical difference of LS before and after modification were analyzed by FT-IR and ^{1}H NMR characterization. The results showed that CL and QLS appear with the same peaks at 3450, 1040, and 2950 cm^{-1} respectively, which are caused by the stretching vibration of −OH, −CO, and −CH, and QLS has a peak at 1470 cm^{-1}, corresponding to the characteristic peak of the quaternary ammonium group (Figure 2a). ^{1}H NMR results showed that QLS had a new peak in chemical shift 3.10 ppm, which is the signal of N−CH$_3$, indicating the success of quaternization modification (Figure 2b).[35] In addition, the characteristic peaks at 1260 and 1545 cm^{-1} in FT-IR correspond to the amide group of chitosan (Figure 2a).[36] The characteristic peak at 1045 cm^{-1} belongs to the absorption peak of S═O, indicating the existence of lignosulfonate sodium in CL. Moreover, compared with LS and CS, CL has a new peak at 1075 cm^{-1}, which is the characteristic stretching vibration peak of C−O, indicating that the hydroxyl group of chitosan or lignin was cross-linked with the aldehyde group of glutaraldehyde. The results confirmed the formation of polymer networks. Figure 2c,d show the C 1s spectra analysis of CS and CL, respectively. The C 1s peak can be deconvoluted into four components, namely, C═O (288 eV), C−O (286.5 eV), C−N (285.9 eV), and C−C/C═C (284.8 eV). Compared with CS, the C−C/C═C peak of CL was significantly enhanced, which was the addition of lignin with high C−C/C═C content. The N 1s spectrum was attributable to the peaks of −NH$_2$ (399 eV) and −NH$_2^+$

https://doi.org/10.1021/cbe.3c00121
Chem Bio Eng. 2024, 1, 252−263

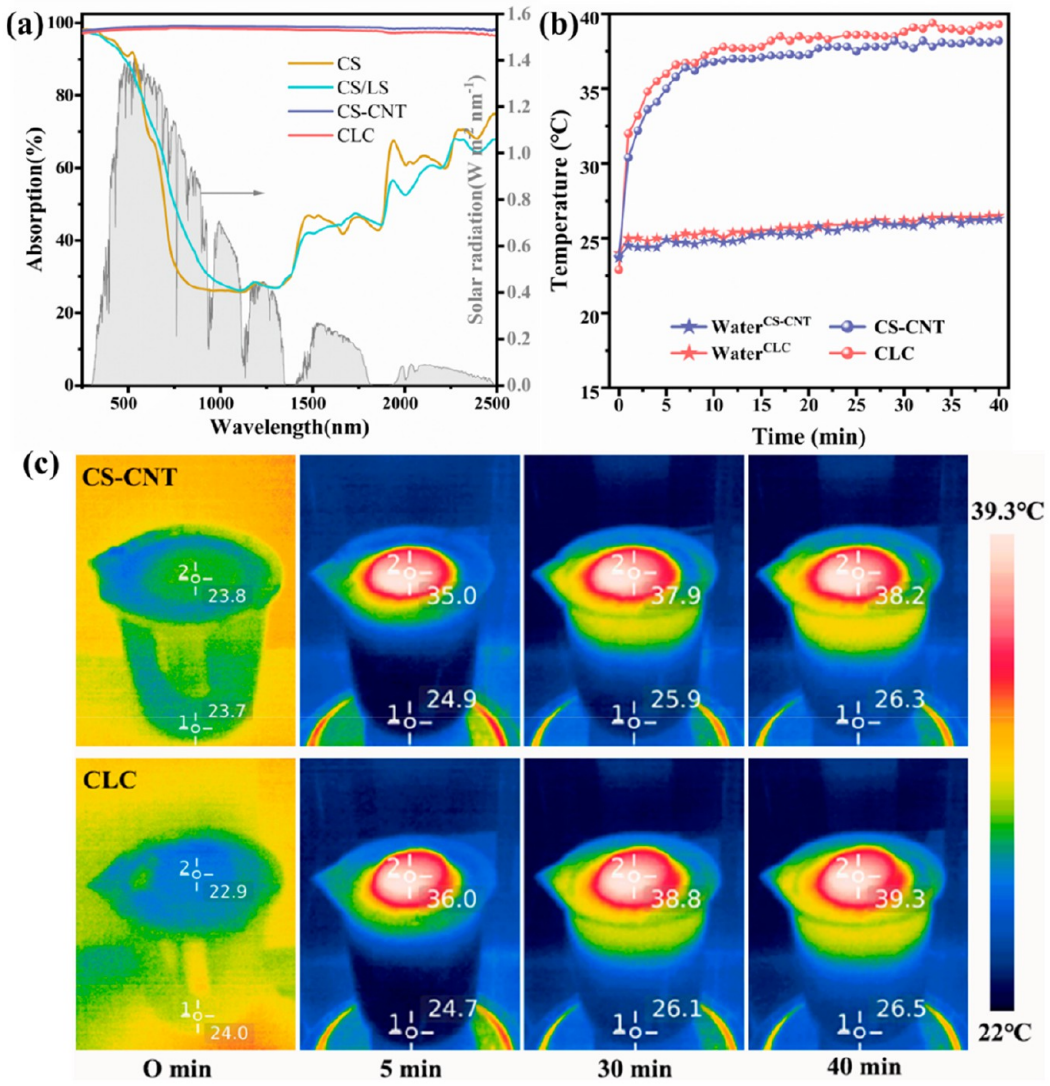

Figure 5. (a) UV−vis−NIR spectra of evaporator and the normalized spectral solar irradiance density of air mass 1.5 global (AM 1.5 G) tilt solar spectrum. (b) The temperatures at CS-CNT and CLC evaporator surfaces and bulk waters under one sun irradiation. (c) The corresponding infrared images at irradiation times of 0, 5, 30, and 40 min, respectively.

(401.9 eV) (Figure 2e,f). In the N 1s spectrum of CL, it was found that the intensity of the $-NH_2^+$ peak, a bonded amino group, increased obviously, indicating that the oxygen-containing functional groups had interacted between chitosan and lignin. Based on the characterization results of FT-IR and XPS, the successful composite of chitosan and lignin was confirmed.

The mechanical properties of hydrogel were analyzed by a rheological instrument, which revealed its viscoelastic properties by the change of modulus. It can be seen from Figure 3a that the storage modulus of CS is 30 Pa. The strain of CS reaches approximately 800% before the sol behavior appears, indicating excellent viscoelasticity. The storage modulus of the CL hydrogel can reach 200 Pa, which is 6.7 times that of CS, indicating that lignin has excellent mechanical strength and can improve the structural stiffness of chitosan hydrogels. At the same time, the storage modulus of the CLC hydrogel reached 812 Pa with the introduction of CNT, which further improved the mechanical strength of the material. In addition, the compression properties of the hydrogel were characterized and analyzed to investigate the mechanical strength of the samples (Figure 3b). The compressive strength of the CL hydrogel is 150 kPa, which is obviously stronger than that of CS (100 kPa), indicating that the introduction of lignin significantly enhances the compressive strength of the hydrogel. Although the flexibility of CS-CNT and CLC is poor after the addition of CNT, the presence of lignin gave the hydrogel excellent compressive strength (192 kPa). Excellent hydrophilicity is also crucial to ensure continuous water transport to the evaporator surface, thereby facilitating water vaporization. As shown in Figure 3c, the water contact angles (WCAs) of CS and CL are 78° and 79°, respectively. The WCAs of CS-CNT and CLC are 81° and 82°, respectively. Although the contact angle increases slightly after doping with hydrophobic CNT, the combination or doping of lignin or CNT did not significantly reduce the hydrophilicity of the hydrogel evaporators. The hydrogel evaporators exhibited hydrophilicity because of the loose porous structure of the hydrogel, with rich interconnected pores facilitating capillary action, enabling easy water absorption.[37] At the same time, the residence time of water droplets on the surface of CLC was observed by the dynamic contact angle. It can be seen from Figure 3d that the

https://doi.org/10.1021/cbe.3c00121
Chem Bio Eng. 2024, 1, 252−263

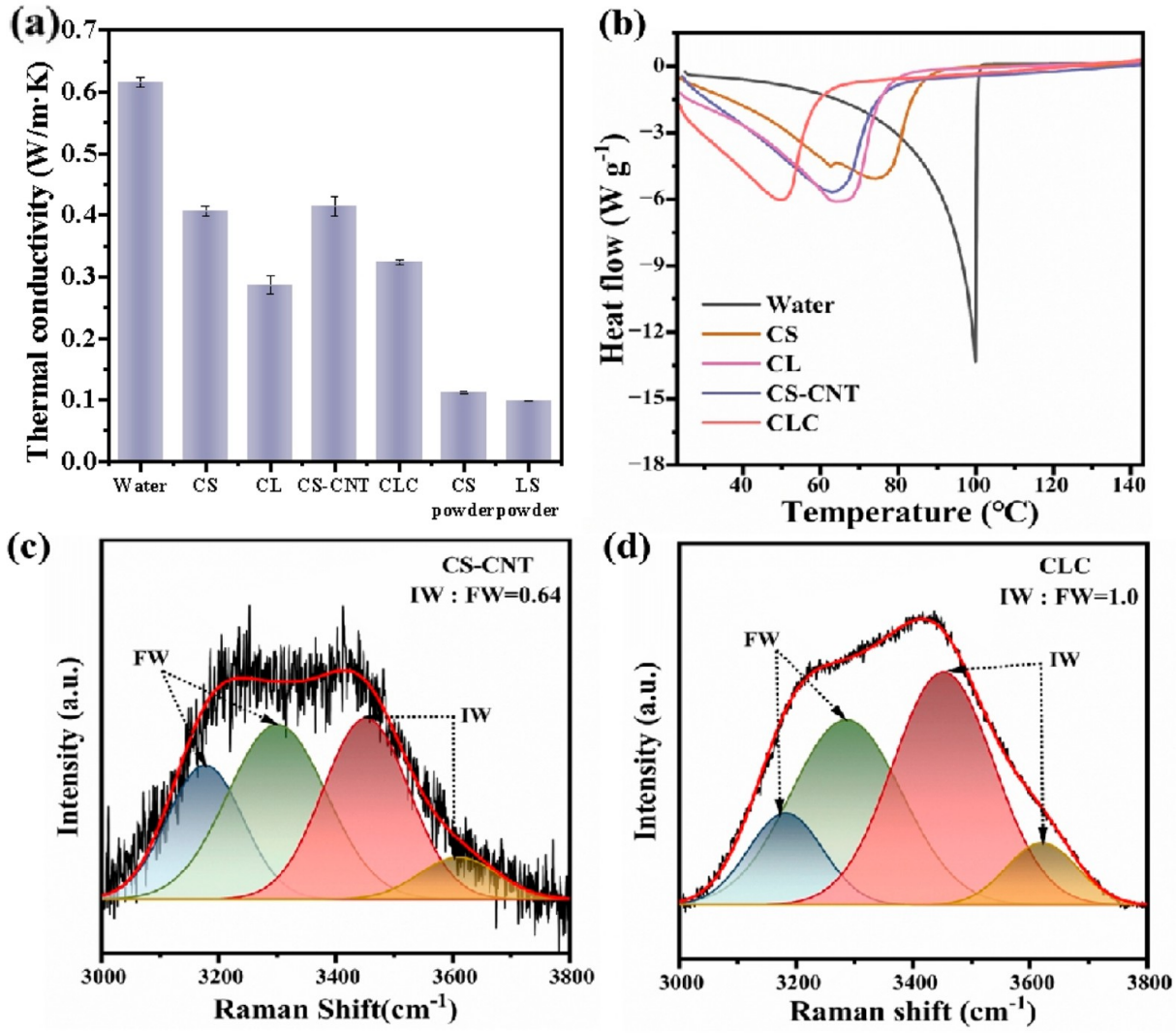

Figure 6. (a) Thermal conductivity of pure water, CS powder, LS powder, and hydrogel in the wet states. (b) DSC curves. Fitting curves are based on the Gaussian function in the energy region of the O−H stretching modes of water in the hydrogel of (c) CS-CNT and (d) CLC hydrogel.

rapid absorption of the water droplets by the CLC hydrogel within 80 ms, indicating its outstanding hydrophilicity. This remarkable hydrophilicity ensures stable water supply characteristics of the CLC evaporator during long-term continuous water evaporation.

3.2. Effect of Preparation Conditions on Evaporation Performance of the CLC Hydrogel. To obtain the best performance of the hydrogel evaporator, the influence of hydrogel preparation conditions was investigated. Under the sunlight intensity of 1 kW m^{-2}, the evaporation rates of different hydrogel samples with the same CNT content were compared. The water evaporation rates of CS, CL, CS-CNT, and CLC are 1.20, 1.90, 2.12, and 2.48 kg m^{-2} h^{-1}, respectively (Figure 4a). By comparison, the addition of lignin and CNT significantly improved the interfacial solar steam generation performance of the hydrogel evaporator. More obviously, the water evaporation rate of CLC is about 6.2 times higher than that of the natural evaporation of water (0.4 kg m^{-2} h^{-1}), indicating that the CLC hydrogel is a potential candidate in interfacial solar steam generation. The effect and function of LS were investigated by changing the proportion in CL (Figure 4b). With the increase in the proportion of LS, the water evaporation rate of the CL hydrogel continues to increase, reaching 2.12 kg m^{-2} h^{-1}. This increase is primarily attributed to the photothermal effect of lignin. The molecular structure of lignin with strong $\pi-\pi$ stacking can promote nonradiative migration and trigger photothermal conversion and then convert light energy into heat energy and release energy in the form of heat energy. Then, CNT was used as a photothermal material to explore the effect of LS on CLC (Figure 4c). The optimal proportion of LS in CLC is 1 wt %, which can endow the evaporation rate of 2.48 kg m^{-2} h^{-1}. Compared with the CL hydrogel, the evaporation performance of the CLC hydrogel is significantly enhanced owing to the substantial photothermal effect of carbon nanotubes.

However, compared with the evaporation performance of CS-CNT, the LS composition in the CLC hydrogel still plays a role similar to that of photothermal materials. Finally, the effect of CNT content on the evaporation rate of hydrogel was investigated in the range 25−100 mg (Figure 4d). Under the CNT dosage of 75 mg (~0.5 wt %), the evaporation rate of CLC reached the maximum of 2.48 kg m^{-2} h^{-1}. However, as the amount of CNT increased, the evaporation rate of hydrogel decreased, which is due to the excessive agglomer-

https://doi.org/10.1021/cbe.3c00121
Chem Bio Eng. 2024, 1, 252−263

ation and accumulation of CNT within the pores, which leads to pore blockage and consequently weakens the water transport capacity.

3.3. Photothermal Effect of the CLC Hydrogel. The solar absorption characteristics of hydrogels were investigated by ultraviolet−visible−near-infrared spectroscopy (UV−vis−NIR) in a wide wavelength range of 250−2500 nm. As shown in Figure 5a, the solar absorption of both CL and CS is 53%. The results showed that the absorption of sunlight by chitosan hydrogel could not be enhanced by incorporation of LS. In addition, the addition of CNT made the CLC hydrogel exhibit excellent broadband solar absorption (97%). The high solar energy absorption rate is one of the crucial factors to improve the solar interface evaporation. The presence of CNT ensures that the CLC hydrogel can maximize the absorption of solar energy and convert it into heat during the process of solar interface evaporation. Infrared thermal imaging was employed to directly monitor the temperature variety of the hydrogel in the process of interfacial solar steam generation (Figure 5b). The heating rate of the CLC hydrogel is fast, from 22.9 to 36 °C in 5 min. The maximum temperature of the top surface in the CLC hydrogel is 39.3 °C under 40 min, while the water temperature of the bottom is 26.5 °C. However, the temperature of the CS-CNT hydrogel only increased to 38.2 °C over 40 min, and the temperature of water reached 26.3 °C, which was slight lower than that of CLC. Under one sun illumination, the CLC hydrogel reached a higher temperature faster, it may be attributed to the presence of lignin reducing the thermal conductivity of CLC hydrogel and the radiation of heat to water, thereby making CLC have better photothermal management ability than CS-CNT. In order to verify the above conjecture, the thermal conductivity of hydrogel in the wet state was investigated by transient hot wire method (Figure 6a). The thermal conductivity of hydrogels was in the range 0.28−0.41 W m^{-1} K^{-1}, which is lower than that of pure water (0.62 W m^{-1} K^{-1}). Compared with CS and CS-CNT hydrogels, CL and CLC hydrogels showed lower thermal conductivity, which proved that the composite of LS could reduce the thermal conductivity of the hydrogels. CLC had a low thermal conductivity of 0.32 W m^{-1} K^{-1}, equivalent to 50% of the thermal conductivity of pure water, which promotes better photothermal management and reduces heat loss from the hydrogel to the water. The result confirmed the excellent photothermal management ability of the CLC hydrogel. This conclusion is further supported by the infrared thermal images of the CS-CNT and CLC, as depicted in Figure 5c.

3.4. Evaporation Mechanism and Performance Evaluation of the CLC Hydrogel. The mechanism and properties of solar water evaporation of hydrogels were thoroughly investigated and compared. Calculating the energy conversion efficiency of CLC based on formula 2, the CLC hydrogel exhibited an evaporation rate of 2.48 kg m^{-2} h^{-1} and an energy efficiency of 90% under one sun illumination. The evaporation enthalpy of water in the hydrogel was characterized and analyzed by differential scanning calorimetry (DSC). As shown in Figure 6b, pure water exhibited a high and sharp peak, whereas the hydrogel exhibited a broader peak of heat flux decay. Moreover, the peak of water heat flux in the hydrogel gradually shifted to the left (<100 °C), facilitating water evaporation at low temperatures. The evaporation enthalpies of water in CS, CL, CS-CNT, and CLC hydrogels are 1808, 1650, 1746, and 1261 J g^{-1}, respectively, which are significantly lower than that of pure water (2104 J g^{-1}). The results showed that both chitosan and LS contributed to reducing the evaporation enthalpy of hydrogel. This is likely attributed to the polar functional groups of CS ($-NH_2$) and LS ($-SO_3H$) combining with water through hydrogen bonding or electrostatic interaction to form a hydrated polymer network, which can regulate the state of water and thus reduce the enthalpy of water evaporation.

Hydrated polymer networks can reduce the enthalpy of evaporation of water.[38] In the polymer network of hydrogels, there are three states of water molecules because of the interaction between water and polymer chains, namely, free water (FW), bound water (BW), and intermediate water (IW), respectively. The IW exists between FW and BW, and it interacts weakly with the polymer chain and adjacent water molecules. Compared with BW and FW, IW needs less energy to break the hydrogen bond to complete the evaporation escape, exhibiting a lower evaporation enthalpy.[14] The O−H stretching region in the hydrogel was characterized by Raman spectroscopy to prove the difference in hydrogen bonding between water molecules. The peaks at 3198 and 3323 cm^{-1} are FW with four hydrogen bonds, two protons, and two electron pairs with adjacent water molecules. The peaks at 3452 and 3600 cm^{-1} correspond to weak or non-hydrogen-bonded IW.[39] The intermediate water ratios (IW:FW) of the CS-CNT and CLC hydrogels are 0.64 and 1.0, respectively (Figure 6c,d). The IW:FW ratio of pure water is between 0.2 and 0.29, indicating that both the CS-CNT and CLC hydrogels have higher intermediate water content.[40] The high intermediate water content correlates with a decrease in the evaporation enthalpy of water. This finding aligns with the DSC characterization analysis, indicating that the presence of CS and LS can reduce the evaporation enthalpy of water in the hydrogel. Moreover, the proportion of intermediate water in the CLC hydrogel reached 1.0, which was 3.4−5 times higher than that of pure water. This elevated intermediate water ratio facilitates water molecules to evaporate and escape with less energy, consequently reducing the evaporation enthalpy of water, lowering the energy required for water evaporation, and enhancing the efficiency of solar energy utilization, thereby leading to a higher evaporation rate.

High solar energy absorption, good thermal management capabilities, and reduced enthalpy of water evaporation contribute to the excellent evaporation performance of the CLC hydrogel. The evaporation performance of the CLC hydrogel including the evaporation rate and energy efficiency were compared with current reports (Figure 7). Compared with chitosan-based hydrogels, the CLC hydrogel achieved higher evaporation properties, surpassing reduced graphene oxide coated chitosan hydrogels (CS-rGO, 1.44 kg m^{-2} h^{-1}),[41] chitosan-tungsten disulfide co-assembled hydrogels (CS-WS_2, 2.10 kg m^{-2} h^{-1}),[42] polydopamine modified Ti_2O_3 nanoparticles and carbon nanotube-chitosan/PVA hydrogels (CS/PVA−PDA/Ti_2O_3/CNT, 1.81 kg m^{-2} h^{-1}),[43] and poly(*N*-acryloyl glycinamide)/chitosan-carbon nanotube hydrogels (PNAGA/CS-CNT, 2.42 kg m^{-2} h^{-1}).[44] At the same time, compared with the current researches on the application of lignin in ISSG, the CLC hydrogel also exhibited excellent properties, surpassing lignin nanoparticle doped PVA hydrogel (PVA-LNPs, 1.62 kg m^{-2} h^{-1}),[45] PVA/LS-carbon nanotube (PVA/LS-CNT, 2.09 kg m^{-2} h^{-1}),[30] and poly(*N*-isopropylacrylamide)/lignosulfonate sodium-polypyrrole (PNIAM/LS-PPy, 2.25 kg m^{-2} h^{-1}).[46] Therefore, the CLC composite hydrogel prepared in this work achieved superior evaporation

https://doi.org/10.1021/cbe.3c00121
Chem Bio Eng. 2024, 1, 252−263

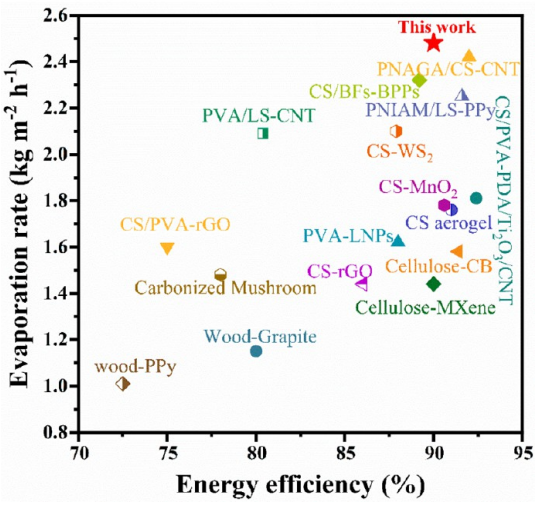

Figure 7. Comparison of the water evaporation rates and energy efficiencies with previously reported chitosan-based/biomass-based or lignin-based hydrogels under one sun irradiation.

performance compared with the reported chitosan-based hydrogels and lignin-based hydrogels.

3.5. Photothermal Antibacterial Properties of the CLC Hydrogel. In the process of water treatment, the elimination of bacteria in water is very important to improve the quality of fresh water and prevent biological pollution on the surface of materials.[47] Staphylococcus aureus was used to explore the antibacterial properties of the hydrogel, while the colonies on Agar plate without hydrogel sample were taken as the control group. As shown in Figure 8a, the antibacterial ratio of the CS, CL, and CLC hydrogels against *Staphylococcus aureus* were 23.4%, 25.4%, and 98.4%, respectively. Figure 8b shows the optical image of the actual bacterial colony number of the sample, which showed that the colony number of the CLC hydrogel decreases obviously. The live/dead staining method was used to explore the antibacterial effect of the hydrogel (Figure 8c). All living bacteria were found in the blank experiments, most bacteria were found alive in the CS and CL hydrogel,[48] while most were found inactivate in the CLC hydrogel. It is proven that the CLC hydrogel can effectively kill bacteria on the surface of hydrogel under one

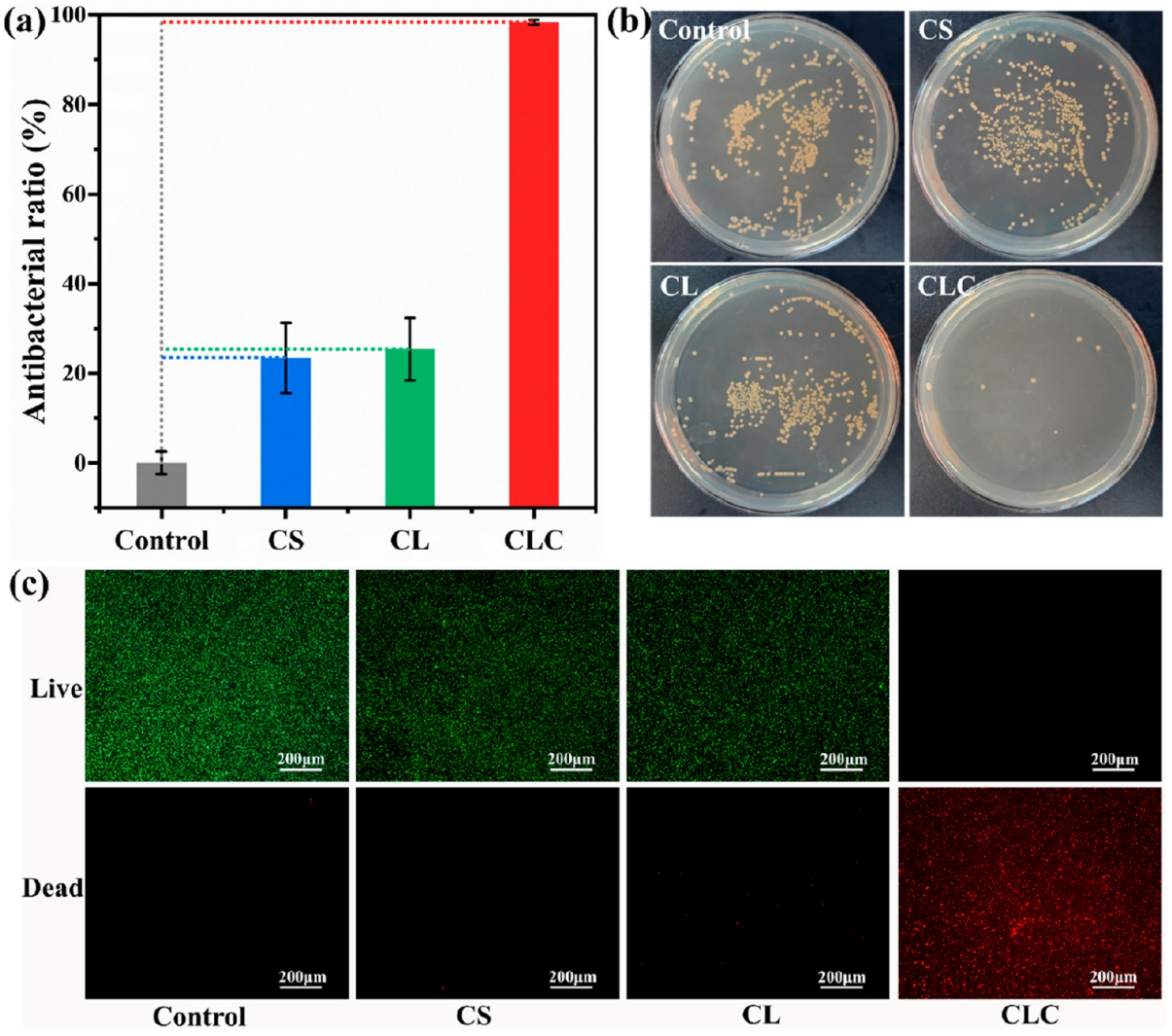

Figure 8. (a) Antibacterial ratio of the CS, CL, and CLC hydrogels to *Staphylococcus aureus*. (b) Optical images of agar plates with bacterial colony forming units. (c) Fluorescence microscopy images of bacteria.

https://doi.org/10.1021/cbe.3c00121
Chem Bio Eng. 2024, 1, 252−263

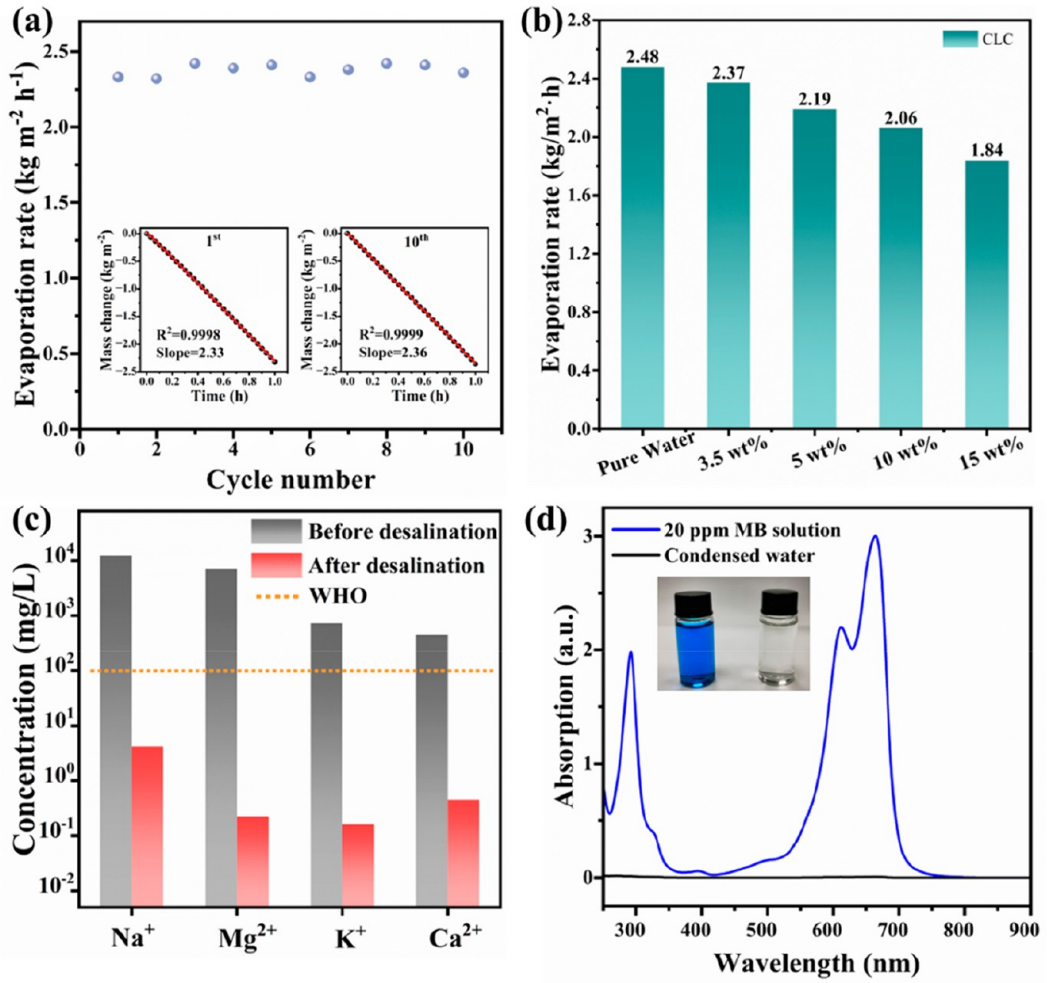

Figure 9. (a) Water evaporation stability of CLC in standard seawater for 10 cycles under one sun of irradiation. The insets show the water mass changes in the 1st and 10th cycles. (b) Water evaporation performance of CLC at different salt concentrations. (c)The measured concentrations of four primary ions in a standard seawater sample before (original) and after desalination. (d) Purification performance of CLC for a sample containing MB.

sun illumination, which can disinfect bacteria in seawater or prevent scaling on the surface of hydrogel.

3.6. Salt Resistance and Long-Term Stability of CLC. The stability of the CLC hydrogel is important in ISSG. Under natural sunlight irradiation, the evaporation performance of the CLC hydrogel was tested for 10 cycles (1 cycle = 1 h) under simulated seawater (Figure 9a). The average evaporation rate of CLC in seawater for 10 cycles is 2.37 kg m^{-2} h^{-1}. The evaporation rate of 10 cycles was basically kept at the same level, indicating that the CLC hydrogel has a stable evaporation rate in seawater. The stable evaporation rate exhibits that the CLC hydrogel has excellent stability in ISSG. The evaporation performance of CLC was evaluated in salt water with a salt concentration of 3.5−15 wt % (Figure 9b). In the salt water with a salt concentration of 3.5 wt %, as a mimic of seawater, the water evaporation rate of the CLC hydrogel is 2.37 kg m^{-2} h^{-1}. When the salt concentration is high (≥ 10 wt %), the evaporation rate of CLC can still be maintained at 2.06−1.84 kg m^{-2} h^{-1}, demonstrating its high evaporation rate in a high salinity environment. These results showed that the CLC hydrogel can continuously evaporate water in seawater for extended periods and exhibits salt tolerance.

Evaluating the water quality of CLC in solar desalination, the concentrations of four main metal ions (Na^+, Mg^{2+}, K^+, and Ca^{2+}) were measured. As shown in Figure 9c, although the salinity in the initial seawater is high, the ion concentration of the desalinated water decreases significantly, demonstrating an excellent desalination rate (>99.96%). In addition, the desalinated water produced by the CLC hydrogel after solar desalination fully met the standard of WHO drinking water standards, confirming the effectiveness of the CLC hydrogel in removing salt from seawater and producing fresh water. Moreover, methylene blue was used to simulate industrial dye wastewater, and the CLC hydrogel exhibited a 100% removal rate, highlighting its exceptional purification capability (Figure 9d). Therefore, the CLC hydrogel prepared in this study holds significant potential for desalinating seawater and treating wastewater to obtain potable water.

4. CONCLUSION

In this work, a straightforward approach to fabricate a chitosan/lignosulfonate sodium−carbon nanotube composite hydrogel for efficient seawater desalination was investigated. The presence of lignosulfonate sodium enhances the mechanical strength of the hydrogel and maintains a stable

https://doi.org/10.1021/cbe.3c00121
Chem Bio Eng. 2024, 1, 252−263

pore structure, ensuring sufficient water transport for evaporation. The interaction between the hydrophilic functional groups in the hydrogels and water promotes the formation of intermediate water, reducing the evaporation enthalpy of water and achieving a high evaporation rate. The evaporation rate of the CLC hydrogels reaches 2.48 kg m^{-2} h^{-1} under one sun illumination with an energy conversion efficiency of 90%, surpassing the previously reported biomass-based hydrogel evaporators. Moreover, the CLC hydrogel also exhibits good salt tolerance and photothermal antibacterial ability in practical applications. The exceptional performance of the CLC hydrogel, coupled with the production of drinkable desalinated water, underscores its role as a sustainable evaporator, facilitating the high-value utilization of lignin and other biomass resources in interfacial solar steam generation.

AUTHOR INFORMATION

Corresponding Authors

Xuliang Lin − *Guangdong Provincial Laboratory of Chemistry and Fine Chemical Engineering Jieyang Center, Jieyang 515200, China; Guangdong Provincial Key Laboratory of Plant Resources Biorefinery, School of Chemical Engineering and Light Industry, Guangdong University of Technology, Guangzhou 510006, China;* orcid.org/0000-0003-2170-5985; Email: xllin@gdut.edu.cn

Xueqing Qiu − *Guangdong Provincial Laboratory of Chemistry and Fine Chemical Engineering Jieyang Center, Jieyang 515200, China; Guangdong Provincial Key Laboratory of Plant Resources Biorefinery, School of Chemical Engineering and Light Industry, Guangdong University of Technology, Guangzhou 510006, China;* orcid.org/0000-0001-8765-7061; Email: cexqqiu@scut.edu.cn

Authors

Ping Wang − *Guangdong Provincial Laboratory of Chemistry and Fine Chemical Engineering Jieyang Center, Jieyang 515200, China; Guangdong Provincial Key Laboratory of Plant Resources Biorefinery, School of Chemical Engineering and Light Industry, Guangdong University of Technology, Guangzhou 510006, China*

Xianjiao Wang − *Guangdong Provincial Laboratory of Chemistry and Fine Chemical Engineering Jieyang Center, Jieyang 515200, China; Guangdong Provincial Key Laboratory of Plant Resources Biorefinery, School of Chemical Engineering and Light Industry, Guangdong University of Technology, Guangzhou 510006, China*

Xiaofei Wang − *Guangdong Provincial Laboratory of Chemistry and Fine Chemical Engineering Jieyang Center, Jieyang 515200, China; Guangdong Provincial Key Laboratory of Plant Resources Biorefinery, School of Chemical Engineering and Light Industry, Guangdong University of Technology, Guangzhou 510006, China*

Complete contact information is available at: https://pubs.acs.org/10.1021/cbe.3c00121

Notes

The authors declare no competing financial interest.

ACKNOWLEDGMENTS

The authors acknowledge the financial support of the National Natural Science Foundation of China (22038004 and U23A6005).

REFERENCES

(1) Reid, A. J.; Carlson, A. K.; Creed, I. F.; Eliason, E. J.; Gell, P. A.; Johnson, P. T. J.; Kidd, K. A.; MacCormack, T. J.; Olden, J. D.; Ormerod, S. J.; Smol, J. P.; Taylor, W. W.; Tockner, K.; Vermaire, J. C.; Dudgeon, D.; Cooke, S. J. Emerging Threats and Persistent Conservation Challenges for Freshwater Biodiversity. *Biol. Rev.* **2019**, *94* (3), 849−873.

(2) Niu, R.; Ren, J.; Koh, J. J.; Chen, L.; Gong, J.; Qu, J.; Xu, X.; Azadmanjiri, J.; Min, J. Bio-Inspired Sandwich-Structured All-Day-Round Solar Evaporator for Synergistic Clean Water and Electricity Generation. *Adv. Energy Mater.* **2023**, *13* (45), No. 2302451.

(3) Jones, E.; Qadir, M.; van Vliet, M. T. H.; Smakhtin, V.; Kang, S. The State of Desalination and Brine Production: A Global Outlook. *Sci. Total Environ.* **2019**, *657*, 1343−1356.

(4) Liu, Z.; Qing, R.-K.; Xie, A.-Q.; Liu, H.; Zhu, L.; Chen, S. Self-Contained Janus Aerogel with Antifouling and Salt-Rejecting Properties for Stable Solar Evaporation. *ACS Appl. Mater. Interfaces* **2021**, *13* (16), 18829−18837.

(5) Sun, Z.; Wang, J.; Wu, Q.; Wang, Z.; Wang, Z.; Sun, J.; Liu, C.-J. Plasmon Based Double-Layer Hydrogel Device for a Highly Efficient Solar Vapor Generation. *Adv. Funct. Mater.* **2019**, *29* (29), No. 1901312.

(6) Liu, N.; Hao, L.; Zhang, B.; Niu, R.; Gong, J.; Tang, T. Rational Design of High-Performance Bilayer Solar Evaporator by Using Waste Polyester-Derived Porous Carbon-Coated Wood. *ENERGY Environ. Mater.* **2022**, *5* (2), 617−626.

(7) Guo, Y.; Lu, H.; Zhao, F.; Zhou, X.; Shi, W.; Yu, G. Biomass-Derived Hybrid Hydrogel Evaporators for Cost-Effective Solar Water Purification. *Adv. Mater.* **2020**, *32* (11), No. 1907061.

(8) Chen, H.; Ma, H.; Zhang, P.; Wen, Y.; Qu, L.; Li, C. Pristine Titanium Carbide MXene Hydrogel Matrix. *ACS Nano* **2020**, *14* (8), 10471−10479.

(9) Zeng, J.; Wang, Q.; Shi, Y.; Liu, P.; Chen, R. Osmotic Pumping and Salt Rejection by Polyelectrolyte Hydrogel for Continuous Solar Desalination. *Adv. Energy Mater.* **2019**, *9* (38), No. 1900552.

(10) Chen, X.; Wu, Z.; Lai, D.; Zheng, M.; Xu, L.; Huo, J.; Chen, Z.; Yuan, B.; Fu, M.-L. Resilient Biomass-Derived Hydrogel with Tailored Topography for Highly Efficient and Long-Term Solar Evaporation of High-Salinity Brine. *J. Mater. Chem. A* **2020**, *8* (43), 22645−22656.

(11) Xu, T.; Xu, Y.; Wang, J.; Lu, H.; Liu, W.; Wang, J. Sustainable Self-Cleaning Evaporator for Long-Term Solar Desalination Using Gradient Structure Tailored Hydrogel. *Chem. Eng. J.* **2021**, *415*, No. 128893.

(12) Zhou, X.; Guo, Y.; Zhao, F.; Yu, G. Hydrogels as an Emerging Material Platform for Solar Water Purification. *Acc. Chem. Res.* **2019**, *52* (11), 3244−3253.

(13) Chu, A.; Yang, M.; Chen, J.; Zhao, J.; Fang, J.; Yang, Z.; Li, H. Biomass-Enhanced Janus Sponge-like Hydrogel with Salt Resistance and High Strength for Efficient Solar Desalination. *Green Energy Environ.* **2023**, DOI: 10.1016/j.gee.2023.04.003.

(14) Guo, Y.; Yu, G. Engineering Hydrogels for Efficient Solar Desalination and Water Purification. *Acc. Mater. Res.* **2021**, *2* (5), 374−384.

(15) Lin, X.; Wang, P.; Hong, R.; Zhu, X.; Liu, Y.; Pan, X.; Qiu, X.; Qin, Y. Fully Lignocellulosic Biomass-Based Double-Layered Porous Hydrogel for Efficient Solar Steam Generation. *Adv. Funct. Mater.* **2022**, *32* (51), No. 2209262.

(16) Sharshir, S. W.; Algazzar, A. M.; Elmaadawy, K. A.; Kandeal, A. W.; Elkadeem, M. R.; Arunkumar, T.; Zang, J.; Yang, N. New Hydrogel Materials for Improving Solar Water Evaporation, Desalination and Wastewater Treatment: A Review. *Desalination* **2020**, *491*, No. 114564.

(17) Zhou, X.; Guo, Y.; Zhao, F.; Shi, W.; Yu, G. Topology-Controlled Hydration of Polymer Network in Hydrogels for Solar-Driven Wastewater Treatment. *Adv. Mater.* **2020**, *32* (52), No. 2007012.
(18) He, P.; Lan, H.; Bai, H.; Zhu, Y.; Fan, Z.; Liu, J.; Liu, L.; Niu, R.; Dong, Z.; Gong, J. Rational Construction of "All-in-One" Metal-Organic Framework for Integrated Solar Steam Generation and Advanced Oxidation Process. *Appl. Catal. B Environ.* **2023**, *337*, No. 123001.
(19) Guo, Y.; Dundas, C. M.; Zhou, X.; Johnston, K. P.; Yu, G. Molecular Engineering of Hydrogels for Rapid Water Disinfection and Sustainable Solar Vapor Generation. *Adv. Mater.* **2021**, *33* (35), No. 2102994.
(20) Do, N. H. N.; Truong, Q. T.; Le, P. K.; Ha, A. C. Recent Developments in Chitosan Hydrogels Carrying Natural Bioactive Compounds. *Carbohydr. Polym.* **2022**, *294*, No. 119726.
(21) Rico-García, D.; Ruiz-Rubio, L.; Pérez-Alvarez, L.; Hernández-Olmos, S. L.; Guerrero-Ramírez, G. L.; Vilas-Vilela, J. L. Lignin-Based Hydrogels: Synthesis and Applications. *Polymers* **2020**, *12* (1), 81.
(22) Lin, X.; Fei, X.; Chen, D.; Qi, Y.; Xu, Q.; Liu, Y.; Zhang, Q.; Li, S.; Wang, T.; Qin, Y.; Qiu, X. Efficient Catalytic Upgrading of Ethanol to Higher Alcohols via Inhibiting C−C Cleavage and Promoting C−C Coupling over Biomass-Derived NiZn@NC Catalysts. *ACS Catal.* **2022**, *12* (19), 11573−11585.
(23) You, X.; Wang, X.; Zhang, H. J.; Cui, K.; Zhang, A.; Wang, L.; Yadav, C.; Li, X. Supertough Lignin Hydrogels with Multienergy Dissipative Structures and Ultrahigh Antioxidative Activities. *ACS Appl. Mater. Interfaces* **2020**, *12* (35), 39892−39901.
(24) Culebras, M.; Barrett, A.; Pishnamazi, M.; Walker, G. M.; Collins, M. N. Wood-Derived Hydrogels as a Platform for Drug-Release Systems. *ACS Sustain. Chem. Eng.* **2021**, *9* (6), 2515−2522.
(25) Lin, X.; Liu, J.; Wu, L.; Chen, L.; Qi, Y.; Qiu, Z.; Sun, S.; Dong, H.; Qiu, X.; Qin, Y. In Situ Coupling of Lignin-Derived Carbon-Encapsulated CoFe-CoxN Heterojunction for Oxygen Evolution Reaction. *AIChE J.* **2022**, *68* (10), No. e17785.
(26) Li, J.; Liu, W.; Qiu, X.; Zhao, X.; Chen, Z.; Yan, M.; Fang, Z.; Li, Z.; Tu, Z.; Huang, J. Lignin: A Sustainable Photothermal Block for Smart Elastomers. *Green Chem.* **2022**, *24* (2), 823−836.
(27) Hao, L.; Liu, N.; Bai, H.; He, P.; Niu, R.; Gong, J. High-Performance Solar-Driven Interfacial Evaporation through Molecular Design of Antibacterial, Biomass-Derived Hydrogels. *J. Colloid Interface Sci.* **2022**, *608*, 840−852.
(28) Gehring, J.; Schleheck, D.; Luka, M.; Polarz, S. Aerosol-Synthesis of Mesoporous Organosilica Nanoparticles with Highly Reactive, Superacidic Surfaces Comprising Sulfonic Acid Entities. *Adv. Funct. Mater.* **2014**, *24* (8), 1140−1150.
(29) Upton, B. M.; Kasko, A. M. Strategies for the Conversion of Lignin to High-Value Polymeric Materials: Review and Perspective. *Chem. Rev.* **2016**, *116* (4), 2275−2306.
(30) Qi, Y.; Liu, B.; Qiu, X.; Zeng, X.; Luo, Z.; Wu, W.; Liu, Y.; Chen, L.; Zu, X.; Dong, H.; Lin, X.; Qin, Y. Simultaneous Oxidative Cleavage of Lignin and Reduction of Furfural via Efficient Electrocatalysis by P-Doped $CoMoO_4$. *Adv. Mater.* **2023**, *35* (14), No. 2208284.
(31) Li, R.; Zhang, L.; Shi, L.; Wang, P. MXene Ti_3C_2: An Effective 2D Light-to-Heat Conversion Material. *ACS Nano* **2017**, *11* (4), 3752−3759.
(32) Xu, Y.; Ma, J.; Liu, D.; Xu, H.; Cui, F.; Wang, W. Origami System for Efficient Solar Driven Distillation in Emergency Water Supply. *Chem. Eng. J.* **2019**, *356*, 869−876.
(33) Xu, Y.; Liu, D.; Xiang, H.; Ren, S.; Zhu, Z.; Liu, D.; Xu, H.; Cui, F.; Wang, W. Easily Scaled-up Photo-Thermal Membrane with Structure-Dependent Auto-Cleaning Feature for High-Efficient Solar Desalination. *J. Membr. Sci.* **2019**, *586*, 222−230.
(34) Zhao, L.; Yang, Z.; Wang, J.; Zhou, Y.; Cao, P.; Zhang, J.; Yuan, P.; Zhang, Y.; Li, Q. Boosting Solar-Powered Interfacial Water Evaporation by Architecting 3D Interconnected Polymetric Network in CNT Cellular Structure. *Chem. Eng. J.* **2023**, *451*, No. 138676.
(35) Wang, H.; Lin, W.; Qiu, X.; Fu, F.; Zhong, R.; Liu, W.; Yang, D. In Situ Synthesis of Flowerlike Lignin/ZnO Composite with Excellent UV-Absorption Properties and Its Application in Polyurethane. *ACS Sustain. Chem. Eng.* **2018**, *6* (3), 3696−3705.
(36) Yao, H.; Zhang, P.; Yang, C.; Liao, Q.; Hao, X.; Huang, Y.; Zhang, M.; Wang, X.; Lin, T.; Cheng, H.; Yuan, J.; Qu, L. Janus-Interface Engineering Boosting Solar Steam towards High-Efficiency Water Collection. *Energy Environ. Sci.* **2021**, *14* (10), 5330−5338.
(37) Peng, B.; Lyu, Q.; Li, M.; Du, S.; Zhu, J.; Zhang, L. Phase-Separated Polyzwitterionic Hydrogels with Tunable Sponge-Like Structures for Stable Solar Steam Generation. *Adv. Funct. Mater.* **2023**, *33* (18), No. 2214045.
(38) Guo, Y.; Fang, Z.; Yu, G. Multifunctional Hydrogels for Sustainable Energy and Environment. *Polym. Int.* **2021**, *70* (10), 1425−1432.
(39) Zhu, F.; Wang, L.; Demir, B.; An, M.; Wu, Z. L.; Yin, J.; Xiao, R.; Zheng, Q.; Qian, J. Accelerating Solar Desalination in Brine through Ion Activated Hierarchically Porous Polyion Complex Hydrogels. *Mater. Horiz.* **2020**, *7* (12), 3187−3195.
(40) Li, W.; Tian, X.; Li, X.; Han, S.; Li, C.; Zhai, X.-Z.; Kang, Y.; Yu, Z.-Z. Ultrahigh Solar Steam Generation Rate of a Vertically Aligned Reduced Graphene Oxide Foam Realized by Dynamic Compression. *J. Mater. Chem. A* **2021**, *9* (26), 14859−14867.
(41) Wang, F.; Wei, D.; Li, Y.; Chen, T.; Mu, P.; Sun, H.; Zhu, Z.; Liang, W.; Li, A. Chitosan/Reduced Graphene Oxide-Modified Spacer Fabric as a Salt-Resistant Solar Absorber for Efficient Solar Steam Generation. *J. Mater. Chem. A* **2019**, *7* (31), 18311−18317.
(42) Yuan, Y.; Han, X.; Cai, H.; Yang, K.; Zhang, S.; Li, X.; Zhang, M. Co-Assembled WS_2 Nanosheets/Chitosan Aerogels with Oriented Micro-Channels for Efficient and Sustainable Solar Steam Generation. *ACS Sustain. Chem. Eng.* **2023**, *11* (12), 4643−4651.
(43) Li, W.; Feng, W.; Wu, S.; Wang, W.; Yu, D. Synergy of Photothermal Effect in Integrated 0D Ti2O3 Nanoparticles/1D Carboxylated Carbon Nanotubes for Multifunctional Water Purification. *Sep. Purif. Technol.* **2022**, *292*, No. 120989.
(44) Lu, H.; Li, M.; Wang, X.; Wang, Z.; Pi, M.; Cui, W.; Ran, R. Recyclable Physical Hydrogels as Durable and Efficient Solar-Driven Evaporators. *Chem. Eng. J.* **2022**, *450*, No. 138257.
(45) Zhao, X.; Huang, C.; Xiao, D.; Wang, P.; Luo, X.; Liu, W.; Liu, S.; Li, J.; Li, S.; Chen, Z. Melanin-Inspired Design: Preparing Sustainable Photothermal Materials from Lignin for Energy Generation. *ACS Appl. Mater. Interfaces* **2021**, *13* (6), 7600−7607.
(46) Jiang, S.; Zhang, Z.; Zhou, T.; Duan, S.; Yang, Z.; Ju, Y.; Jia, C.; Lu, X.; Chen, F. Lignin Hydrogel-Based Solar-Driven Evaporator for Cost-Effective and Highly Efficient Water Purification. *Desalination* **2022**, *531*, No. 115706.
(47) Peng, B.; Lyu, Q.; Gao, Y.; Li, M.; Xie, G.; Xie, Z.; Zhang, H.; Ren, J.; Zhu, J.; Zhang, L.; Wang, P. Composite Polyelectrolyte Photothermal Hydrogel with Anti-Biofouling and Antibacterial Properties for the Real-World Application of Solar Steam Generation. *ACS Appl. Mater. Interfaces* **2022**, *14* (14), 16546−16557.
(48) Wu, X.; Cao, S.; Ghim, D.; Jiang, Q.; Singamaneni, S.; Jun, Y.-S. A Thermally Engineered Polydopamine and Bacterial Nanocellulose Bilayer Membrane for Photothermal Membrane Distillation with Bactericidal Capability. *Nano Energy* **2021**, *79*, No. 105353.

https://doi.org/10.1021/cbe.3c00121
Chem Bio Eng. 2024, 1, 252−263